Analysis and test of a wireless impedance-loaded SAW sensor

Xifeng Zhu, Jianchun Xing, Liqiang Xie ✉, *Tianxian Wang*

College of Defense Engineering, Army Engineering University of PLA, Nanjing 210007, People's Republic of China
✉ *E-mail: xielq@outlook.com*

Published in Micro & Nano Letters; Received on 9th July 2018; Revised on 5th December 2018; Accepted on 21st December 2018

Instead of a conventional wireless transceiver system that requires batteries and complex circuits, the surface acoustic wave (SAW) sensor enables wireless passive measurement. A sensor consisting of an SAW device and external impedance sensing element is analysed. Since the reflection coefficient of the reflective grating on the SAW device depends on the load impedance, the echo characteristics are influenced by the change in the impedance of external sensing element. A resistance sensor or a capacitive sensor is selected as the external sensing element. The two different types of sensors are simulated using coupling-of-mode (COM) modelling, and the relationships between amplitude and phase with load impedance are analysed. On the basis of COM theory, a wireless impedance-loaded SAW sensor is fabricated by the lift-off process and tested by a network analyser to verify the simulation results. It is observed that the test results agree well with the simulation results. The phase change is more sensitive than the amplitude based on the results obtained. The sensitivity is 0.274°/Ω for the sensor with resistance and the sensitivity of the sensor with capacitance is 1.096°/pF. These results can guide the design of the high sensitivity impedance-loaded SAW sensors in the future.

1. Introduction: The impedance-loaded surface acoustic wave (SAW) sensor has been widely used in sensing applications taking advantage of its small size, low power consumption, long readout distance, wireless communication and passive operation [1–3]. A schematic diagram of a wireless impedance-loaded SAW sensor is shown as Fig. 1. The sensor consists of an SAW device and an external impedance sensing element. The operating principle of this sensor is described below: a pulse signal from the radio-frequency interrogation unit is sent to the antenna connected to the IDT and converted into an electrical signal. The Interdigital Transducer (IDT) converts the electrical signal into SAW through the reverse piezoelectric effect of the piezoelectric substrate, and part of the SAW is reflected back by the reflective grating on the propagation path. Then, the SAW is converted into an electrical signal by the IDT and the electrical signal is sent to the interrogation unit by the antenna. Since the reflection coefficient of the reflective grating is influenced by the load impedance of external sensing element seriously, the amplitude and phase of the echo wave are highly sensitive to the load impedance of the sensing element. The extraction of the amplitude and phase finally reaches the purpose of wireless passive measurement.

The impedance-loaded sensors are mainly analysed using delta function model, the equivalent circuit model and coupling-of-mode (COM) model [4–7]. However, the delta function model ignores the influence of electrode pairs on the performance of sensors and the equivalent circuit model is complicated to be deduced. The COM model has relatively good flexibility and high accuracy [8] since it takes all factors that affect the parameters of impedance-load SAW sensor into consideration including propagation loss, electrode resistance, distributed capacitance and other second-order effects. Therefore, this Letter uses the COM model to simulate and analyse the performance of the impedance-loaded SAW sensors, and the correctness of COM model analysis is proved by experiment. Moreover, the loaded impedances of the SAW sensors can be resistive or capacitive. Then, the resistive and capacitive impedance-loaded sensors are analysed.

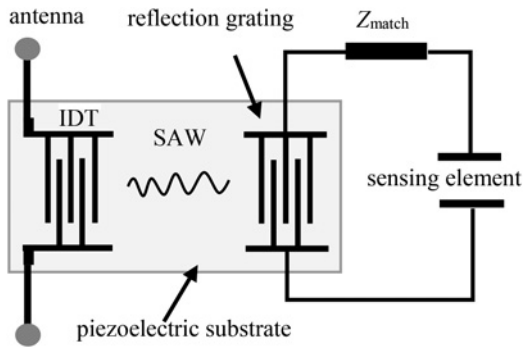

Fig. 1 *Schematic diagram of a wireless impedance-loaded SAW sensor*

2. COM analysis for SAW sensors: The control equation for COM modelling is expressed as [9, 10]

$$\begin{aligned}\frac{\partial U_+(x)}{\partial x} &= -\mathrm{j}\theta_\mathrm{U} U_+(x) - \mathrm{j}kU_-(x) + \mathrm{j}\alpha V \\ \frac{\partial U_-(x)}{\partial x} &= -\mathrm{j}k^* U_+(x) - \mathrm{j}\theta_\mathrm{U} U_-(x) - \mathrm{j}\alpha V \\ \frac{\partial I(x)}{\partial x} &= 2\mathrm{j}\zeta U_+(x) + 2\mathrm{j}\zeta U_-(x) - \mathrm{j}\omega C_\mathrm{s} V \\ \theta_\mathrm{U} &= \frac{2\pi(f - f_0)}{v} - \mathrm{j}\gamma\end{aligned} \tag{1}$$

Here, $U_\pm(x)$ is the amplitudes of the SAW in both forward and reverse directions; V is the voltage applied to the terminal of the IDT; I is the current generated by the IDT; k and α are the coefficients of transduction and reflectivity, respectively; C_s and γ are the static capacitance and propagation loss per unit length, respectively; f_0 is the operating frequency; and v is the velocity of the SAW.

Both IDT and reflective grating are analysed by COM modelling. The COM parameters required in the model are given in Table 1. The solution of the COM equations expressed by the P-matrix for IDT with length L is as follows:

$$\begin{bmatrix} U_-(0) \\ U_+(L) \\ I \end{bmatrix} = \begin{bmatrix} P_{\mathrm{IDT11}} & P_{\mathrm{IDT12}} & P_{\mathrm{IDT13}} \\ P_{\mathrm{IDT21}} & P_{\mathrm{IDT22}} & P_{\mathrm{IDT23}} \\ P_{\mathrm{IDT31}} & P_{\mathrm{IDT23}} & P_{\mathrm{IDT33}} \end{bmatrix} \begin{bmatrix} U_+(0) \\ U_-(L) \\ V \end{bmatrix} \tag{2}$$

In the case of the IDT-type reflective grating with the external sensing element, the total impedance can be written as

$$Z = Z_\mathrm{load} + Z_\mathrm{match} \tag{3}$$

doi: 10.1049/mnl.2018.5375

Table 1 Simulation parameters

Simulation parameters	Value
operating frequency, f_0, MHz	99.5
velocity, v, m/s	3980
Al thickness, nm	1200
Al resistivity, Ωm	27×10^{-9}
reflectivity per wavelength, k	−0.0189
static capacitance per transduction period, C, F/cm	4.5×10^{-12}
electromechanical coupling factor, K^2, %	5.5
propagation loss per unit length, γ, dB/μm	2.5×10^{-4}
propagation path, L, mm	4

where Z_{load} and Z_{match} are the impedances of the external sensing element and matching circuits, respectively. Thus, the P-matrix of it is represented by

$$\begin{bmatrix} U_-(0) \\ U_+(L_r) \\ I \end{bmatrix} = \begin{bmatrix} P_{r11} & P_{r12} & P_{r13} \\ P_{r21} & P_{r22} & P_{r23} \\ P_{r31} & P_{r23} & P_{r33} + 1/(Z_{load} + Z_{match}) \end{bmatrix} \times \begin{bmatrix} U_+(0) \\ U_-(L_r) \\ V \end{bmatrix} \quad (4)$$

The SAW propagating to the edge of the SAW device substrate is absorbed, so that, to prevent it from being reflected back to the IDT to interfere with the device. Therefore, the boundary condition can be obtained and substituted into P-matrix (2) and (4). The total reflection coefficient P_{11t} of the reflective grating connecting the external sensing element can be determined as follows [11, 12]:

$$P_{11t} = P_{11}^{SC} + \frac{2P_{r13}^2}{P_{r33} + 1/(Z_{load} + Z_{match})} \quad (5)$$

where P_{r13} is the transfer function between the electrical port and the acoustic port. P_{r33} and P_{11}^{sc} are the input admittance and the reflection coefficient of the short-circuit reflective grating. According to (5), the reflection coefficient S_{11} of the impedance-loaded SAW sensor can be accurately simulated and calculated.

3. Test for SAW sensors: On the basis of the COM theory, the parameters of SAW device are as follows: the transduction periodicity is set to 40 μm, the number of interdigital electrode pairs for IDT and reflective grating is 30 and their aperture is 4 mm, and the distance between the reflective grating and IDT is designed to be 8 mm. In addition, the SAW device is fabricated by the lift-off process. The schematic diagram of the fabrication process is illustrated in Fig. 2. The AZ5214 positive photoresist with a thickness of 1300 nm is spin coated on the surface of the 128° YX-lithium niobate substrate. The photoresist is selectively ultraviolet exposed using a mask and the unexposed photoresist is removed from the developer to construct IDT and reflective grating patterns. A 1200 nm thick aluminium (Al) layer is deposited by electron beam evaporation. Then, the substrate is placed in an acetone solution to lift off the photoresist and the Al layer on it. The metal electrode pattern in close contact with the substrate is retained. Therefore, the designed SAW device (Fig. 3) can be

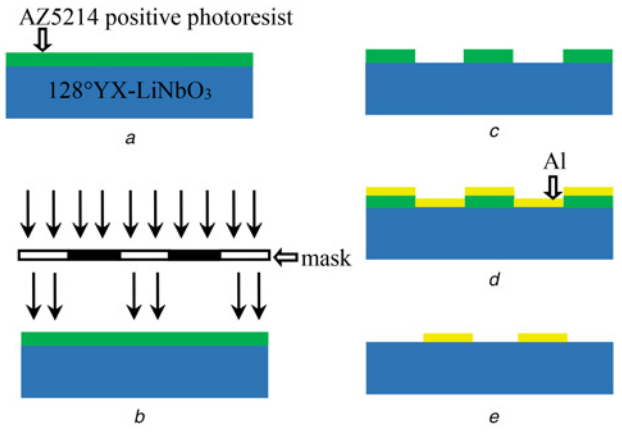

Fig. 2 *Schematic diagram of the fabrication process*
a Photoresist deposition
b Exposure
c Development
d Al deposition
e Lift off

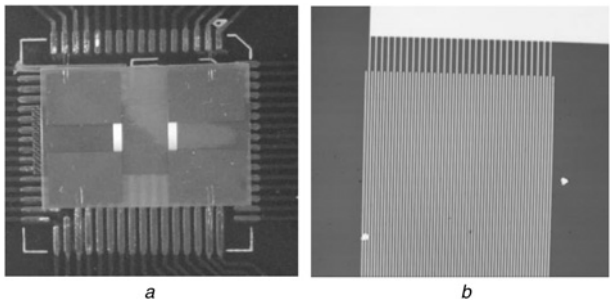

Fig. 3 *Diagram of the fabricated SAW device*
a SAW device with IDT and reflective grating
b Electrode pairs of IDT and reflective grating

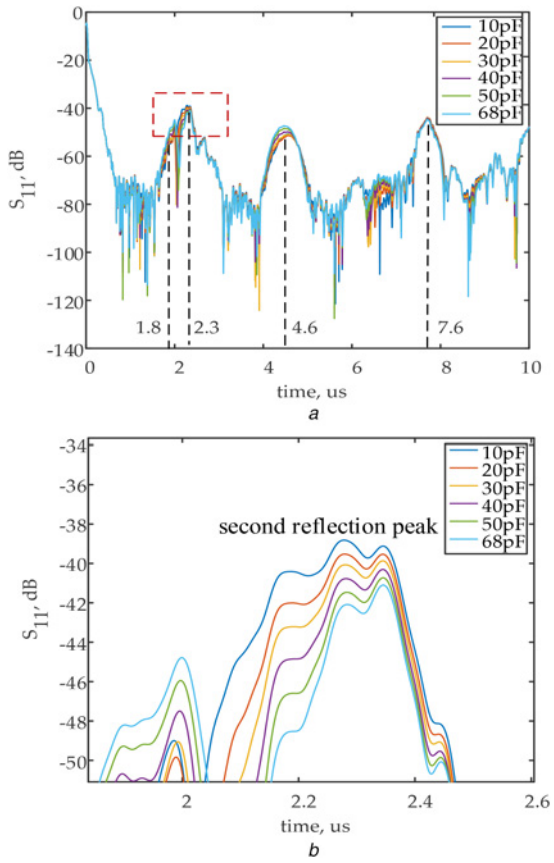

Fig. 4 *Test results with the capacitive sensor*
a Measured S_{11} in the time domain varies with the capacitance from 10 to 68 pF
b Change in S_{11} of the second reflection peak in Fig. 4*a* (the partial enlargement of the second reflection peak)

fabricated through the above process. Moreover, the network analyser is used to measure the echo characteristics of the impedance-loaded sensor.

4. Results and discussion: Two different types of sensors, capacitive sensor and resistance sensor, are applied to external sensing elements. The variable capacitor and the variable resistor are taken as the impedances of the external capacitance sensor and the resistance sensor, respectively.

The manufactured SAW sensor is tested and the measured time domain is presented in Fig. 4*a*. It can be seen that there are four reflection peaks. The first and the fourth reflection peaks present at 1.8 and 7.6 µs, which is matched with the distances 3.6 and 15 mm from the IDT to the edges of the SAW device. Then, the first and the fourth reflection peaks are considered to be the results of the edge reflecting effect.

To eliminate the effects of the edge effect, we can use the absorber near the edge or tilt the edge. The second reflection peak is observed at 2.3 µs. This is obtained by the reflection of the grating which connects with the external sensing element. The third reflected peak observed at 4.6 µs is considered to be caused by the secondary reflection of SAW.

4.1. Capacitive sensor: The ceramic capacitors in the range of 10–68 pF are used to simulate the impedance of the capacitive sensor. As shown in Fig. 4*b*, the characteristic of the second reflection peak is significantly changed as the applied capacitance increases since the artificially applied capacitance changes the load impedance of the matching impedance circuit.

The amplitude and phase change of the second reflection peak is shown in Figs. 5*a* and *b*. It can be observed that the amplitude and capacitance are linearly related, while the phase and capacitance are nonlinear. The amplitude is decreased by 5.548 dB in the range of 10–68 pF. The sensitivity is 0.096 dB/pF. The phase in the same range of capacitance changes by 33.72°, when the capacitance range is 10–30 pF, the phase change is obvious, and the phase and capacitance are almost linearly related; moreover, in the range of 30–68 pF, the slope of the phase change is smaller. To achieve the best sensitivity, 10–30 pF is selected as the sensitive range of phase. The sensitivity is 1.096°/pF. It is clear that phase changes are more sensitive than amplitude. The simulation is carried out by COM modelling and impedance matching in order to verify the rationality of the test results. As shown in Fig. 5, the simulation results are not in well-agreement with the measurement results by comparing the simulation results with the test results. The maximum differences between simulation and measurement results of amplitude and phase are 0.8 dB and 5.21°, respectively. This is because the environmental impact of the test process is hard to be simulated, and the impedance of the SAW device is difficult to match the measurement unit accurately. It is also because the SAW device is small in size and slight inaccuracies in the manufacturing process will result in large variations in the results. Simultaneously, the inaccurate simulation parameters can also cause the deviations between the simulation and the measurement results. These differences are within the allowable range. Therefore, the measurement results are reasonable and credible.

4.2. Resistance sensor: The other type of sensing elements for impedance-loaded SAW sensor is a resistive sensor and the resistance varies from 10 to 62 Ω. The time-domain diagram of the

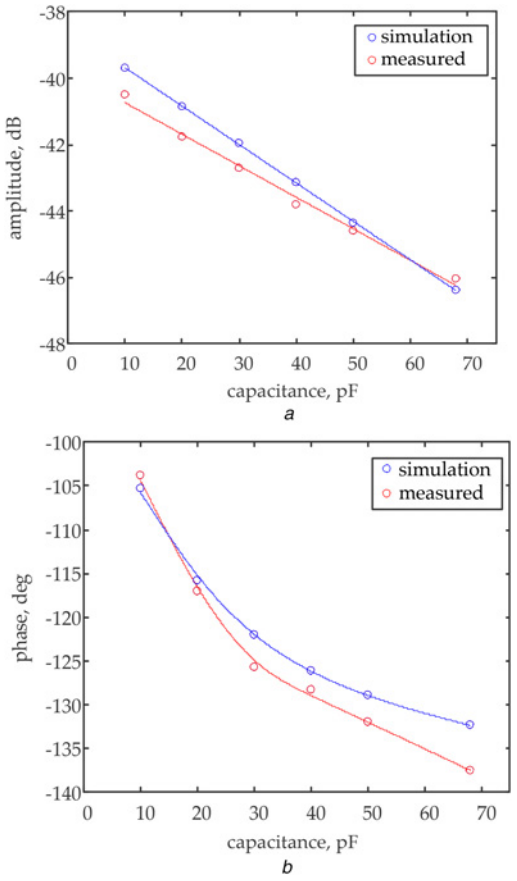

Fig. 5 *Amplitude and phase change with capacitance*
a Echo amplitude with varying capacitance
b Echo phase with varying capacitance

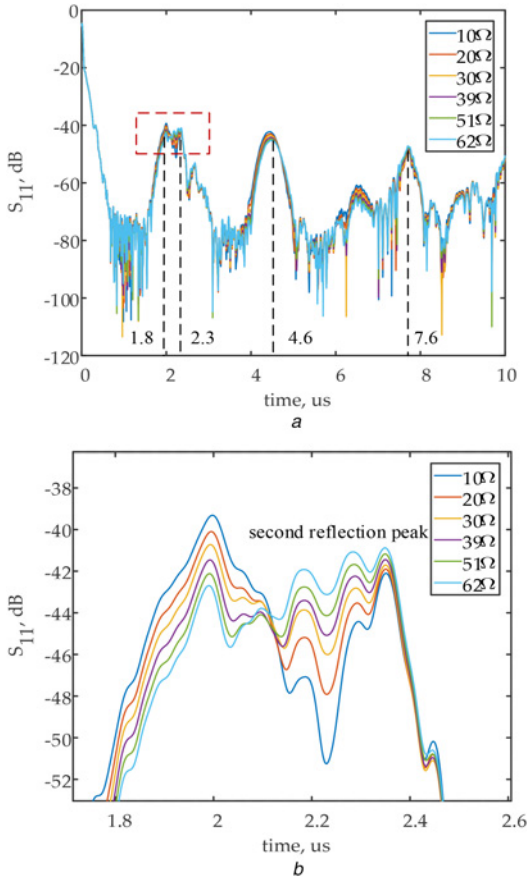

Fig. 6 *Test results with resistance sensor*
a Measured S_{11} in the time domain varies with the resistance from 10 to 62 Ω
b Change in S_{11} of the second reflection peak in Fig. 6*a* (the partial enlargement of the second reflection peak)

doi: 10.1049/mnl.2018.5375

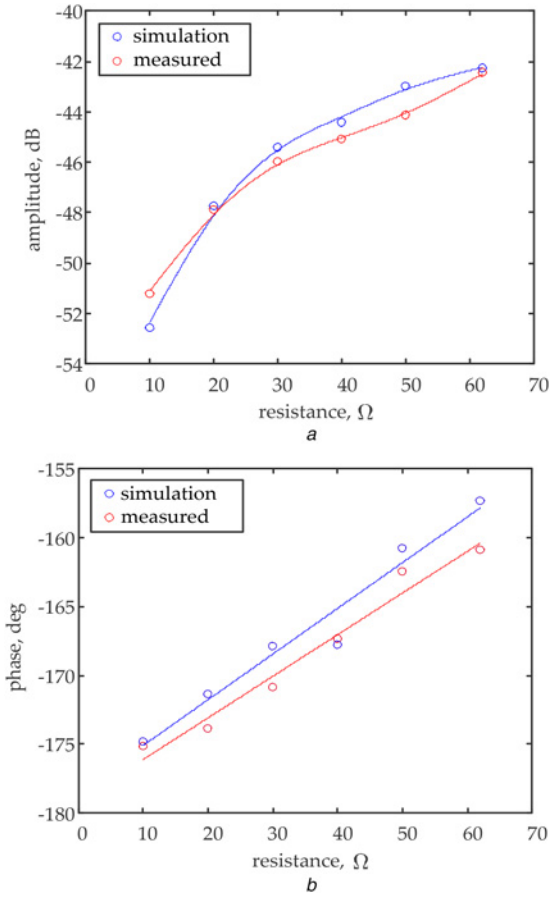

Fig. 7 *Amplitude and phase change with resistance*
a Echo amplitude with varying resistance
b Echo phase with varying resistance

different resistors tested by experiments is shown in Fig. 6. It is observed that the echo amplitude increases as the resistance increases. The incremental change in amplitude is redrawn to determine the sensitivity between amplitude and resistance, as shown in Fig. 7*a*. They are nonlinearly related and the amplitude varies 8.793 dB. When the resistance range is 10–30 Ω, the amplitude changes significantly and is almost linearly related to resistance, thus 10–30 Ω is selected as the sensitive range of the amplitude and the sensitivity is 0.233 dB/Ω. Meanwhile, the echo phase also changes with varying resistance. Fig. 7*b* shows the relationships between phase and resistance. Good linearity and sensitivity are observed. In the same range of resistance changes, the phase increases 14.24° and the sensitivity is 0.274°/Ω. The average difference between simulation and measurement results of amplitude and phase is 0.223 dB and 1.772°, respectively. These differences can be negligible due to the instability of the measurement environment. Therefore, it can be considered that the measurement results are in good agreement with the simulation results.

5. Conclusion: A wireless impedance-loaded SAW sensor is analysed and tested in order to obtain large amplitude modulation and high sensitivity. The SAW sensors with different loads are simulated by COM modelling. Then, we further analyse the relationships between the amplitude and phase with the load impedance. Furthermore, in order to verify the accuracy of the simulation results, we fabricate the designed SAW sensor through the lift-off process and test it with the Agilent E5063A network analyser. The research shows that the test results are consistent with the simulation results. Moreover, the result indicates the phase change is more sensitive than the amplitude. The phase change is more sensitive than the amplitude based on the results obtained. The sensitivity is 0.274°/Ω for the sensor with resistance and the sensitivity of the sensor with capacitance is 1.096°/pF. These results can guide the design of the high sensitivity impedance-loaded SAW sensors in the future.

6. Acknowledgments: This work was supported by the National Natural Science Foundation of China (grant no. 51505499) and the Jiangsu Province Natural Science Foundation of China (grant no. BK20150712).

7 References

[1] Stoney R., Donohoe B., Geraghty D., *ET AL.*: 'The development of surface acoustic wave sensors (SAWs) for process monitoring', *Procedia CIRP*, 2012, **1**, pp. 569–574
[2] Morgan D.: 'Surface acoustic wave filters: with applications to electronic communications and signal processing' (Academic Press, Oxford, UK, 2010)
[3] Kondoh J., Sato H., Oishi M.: 'Vibration characteristics measurements of damaged cantilever using impedance-loaded SAW sensor'. 2016 IEEE Int. Ultrasonics Symp. (IUS), Tours, France, 2016
[4] Hashimoto K.: 'Analysis of excitation and propagation of acoustic waves under periodic metallic-grating structure for SAW device modeling'. Proc. IEEE Ultrasonics Symp., Baltimore, USA, 1993
[5] Kojima T., Shibayama K.: 'An analysis of an equivalent circuit model for an interdigital surface-acoustic-wave transducer', *Jpn. J. Appl. Phys.*, 1988, **27**, (S1), p. 163
[6] Genji T., Kondoh J.: 'Analysis of passive surface acoustic wave sensors using coupling of modes theory', *Jpn. J. Appl. Phys.*, 2014, **53**, (7S), p. 07KD02
[7] Priya R.B., Venkatesan T., Pandya H.M.: 'A comparison of surface acoustic wave (SAW) delay line modelling techniques for sensor applications', *J. Environ. Nanotechnol.*, 2016, **5**, (2), pp. 42–47
[8] Hashimoto K.: 'Acoustic wave devices in telecommunications: modelling and simulation' (Springer, New York, 2000)
[9] Jung I.K., Chen F., Lee K.K.: 'Chipless wireless neural probes based on one-port surface acoustic wave delay line and neural-firing-dependent capacitors', *Jpn. J. Appl. Phys.*, 2014, **53**, (6S), p. 06JM07
[10] Genji T., Kondoh J., Jung I.K., *ET AL.*: 'Measurement of cantilever vibration using impedance-loaded surface acoustic wave sensor', *Jpn. J. Appl. Phys.*, 2016, **55**, p. 07KD06
[11] Genji T., Kondoh J.: 'Analysis of impedance-loaded passive saw sensor'. 2014 IEEE Int. Frequency Control Symp. (FCS), Taipei, Taiwan, 2014
[12] Fu Q., Luo W., Wang Y., *ET AL.*: 'Simulation of wireless passive SAW sensors based on FEM/BEM model'. IEEE Ultrasonics Symp., 2008 IUS 2008, Beijing, China, 2008